Research Square

Preprints are preliminary reports that have not undergone peer review.
They should not be considered conclusive, used to inform clinical practice,
or referenced by the media as validated information.

High Productivity With Laser Beam Splitting in Powder Bed Fusion for Multiple Similar Parts

Florian Joachim Oskar Spieth

florian.spieth@de.bosch.com

Robert Bosch Manufacturing Solutions GmbH

Frederik Henß

Robert Bosch Manufacturing Solutions GmbH

Thorsten Heeling

Robert Bosch Manufacturing Solutions GmbH

Hans-Christian Möhring

University of Stuttgart

Research Article

Keywords:

Posted Date: November 10th, 2026

DOI: https://doi.org/10.21203/rs.3.rs-11366783/v1

License: This work is licensed under a Creative Commons Attribution 4.0 International License.
Read Full License

Additional Declarations: No competing interests reported.

HIGH PRODUCTIVITY WITH LASER BEAM SPLITTING IN POWDER BED FUSION FOR MULTIPLE SIMILAR PARTS

Abstract:

This paper evaluates a highly productive laser-based additive manufacturing process using beam multiplication by investigation of the influences on build quality of 316L stainless-steel parts with different compensation strategies. Many of the current approaches to increase productivity in powder bed fusion with laser beam for metals have resulted in substantial increases in investments for multiple laser-scanner systems or tend to come with the necessity to decrease the quality or resolution of build parts to introduce higher laser power parameter sets. To address these challenges, an alternative approach of increasing the productivity is the use of a beam splitter to build multiple parts simultaneously with a single laser scanner system. While this approach enables higher achievable build rates per laser, it leads to certain differences in the quality-determining properties of the build parts, which are investigated in this work. Therefore, the differences in properties are analysed by density, roughness, and positioning accuracy of the parts. This demonstrates the potential of compensation for optical errors in additive manufacturing with a beam splitter for the purpose of enabling higher productivity to increase the viability of series production for similar parts.

Introduction:

To bring additive manufacturing into series production for high-volume series parts, there is a growing need for more productivity in the additive processes, especially lowering the machine costs and increasing the production efficiency [2,1] In order to deliver higher performance and lower costs over the lifetime of a product, it is further needed to increase the cost competitiveness of metal additive manufacturing (AM) by productivity increases to overcome the entry limits to large-scale investments for a series production [3]. This is especially true for the most commonly used metal additive manufacturing process, powder bed fusion of metals with laser beam (PBF-LB/M), due to its low build rates compared to other metal AM processes [4].With decreasing prices for laser power, one promising way of increasing productivity is to use more power in one machine [5]. The current mainly used ways of doing that are by integrating multiple laser scanner systems in one machine and by optimizing the process to the optimum between productivity and quality. Additionally, further improvements concerning multi laser machines, smaller optics, and improvements in scan strategies are currently researched [6].Although multi-laser machines offer the highest flexibility for processing, the interconnection of areas built by separate lasers in a combined part is still part of research due to differences in the build quality and mechanical properties compared to the areas built by a single laser [7]. Those drawbacks can be compensated in some cases with special exposure strategies for the overlapping areas [9,8]. Another way of using multiple lasers on one powder bed is by positioning the beams in close proximity to each other on the build plate. While this mitigates the risk of locally differing properties for the build part, this close interaction of the laser spots often increases the overall size of the melt pool, which limits its use for smaller features compared to a single beam process. [10,12,11] Nevertheless, in both cases, typically the investment cost for the machine increases due to the additional needed optics and laser sources, and the overlap of the scan fields on the build plate is limited by the scanner sizes [13]. Consequently, this challenge is addressed by the use of higher laser power per single laser scanner system. The maximum deliverable power to the powder bed is typically constrained due to limitations on the scanning speed from the balling effect and the peak intensities arising from the gaussian beams intensity distribution [14,15]. To overcome these limitations, the peak intensity can be reduced with new beam shapes for example the donut profile [16], defocus of a gaussian beam [15] or beam splitting [17,18] while the resulting larger melt pools offer the possibility to use higher scanning speeds by offsetting the Plateau-Rayleigh instability [19]. While this increase in melt pool width leads to higher productivity, it also leads to a loss of feature resolution. All in all, a similar trade-off between productivity and resolution as with larger layer heights arises [21,20]. This leads to the conclusion that for every application with a specific set of quality requirements, size, and production

volume, there is an optimal yet limited number of laser scanner systems and an optimal single beam process. In this case, to further use additionally available laser power and optical headroom, the productivity per laser-scanner system must be increased. While it might be an option to partially lower the investment by adding multiple lasers to one scanner [22] the most prevalent option to do so in PBF-LB/M is the use of a beam splitter to print multiple separate weld beads with one laser scanner system simultaneously. Yet these optical systems use telecentric lenses after the beamsplitter to stop the further propagation of the beams at an angle. While this reduces the optical errors when deflecting the beam on different parts of the build plate, it limits the maximum spot distance. [23,24]. Looking in other fields of laser material processing like laser surface ablation, beam splitting is similarly used to increase the productivity of processes like surface optimisation for tools [25]. In these fields some work is known addressing the optical errors, where the position deviation of multi spot laser drilling process is investigated. The results showed that an optimized optical configuration concerning the f-theta lens and the beam splitter can partially reduce the optical positioning errors. [26] In a subsequent work an active system consisting of two transparent rotating cuboids is successfully tested to further compensate for position errors when deflecting the beams on different positions on the build plate. While this system showed good results in compensating for the position errors, if used, it would add to the necessary optical parts and thereby to the total cost of such a machine. [27]
Nevertheless, the effects of active compensation on optical errors for beam splitting with spot distances larger than 30 mm in a 3d-scanner system is not investigated yet. In order to use beam splitters in PBF-LB/M for separate parts, the compensation of the optical errors has to be improved to allow for larger spot distances on large, fully overlapping scan fields on the build plate, resulting in being able to build larger parts in parallel in the form of hybrid additive manufacturing on conventionally machined substrates. For this specific task, besides the geometric deviations from positioning errors, the focus errors resulting, in different spot diameters on the build plate are seen as both process parameters and optical error values [29,28]. While as a process parameter the spot size is limited by process laser power and minimal feature size, the error value represents a difference in the spots of the different beams.
Therefore, research is necessary to further investigate the resulting differences in build quality and the effects of the compensation framework on simultaneous build parts experimentally manufactured by beam splitting in a 3d-laser scanner system. To compare the effects of the compensation approaches investigated in this work, a consistent set of build-quality criteria is required. Therefore, in this study the build quality is assessed through density measurements, surface roughness measurements, metallographic analysis, and positioning accuracy. Depending on the intended application, particularly in series production, this assessment may be extended to include mechanical properties and further characteristics. Nevertheless, within its initial scope, the study aims to provide first insights into the effects of the compensation approaches on build quality. The broader objective is to increase PBF-LB/M productivity by distributing the power of a single laser among multiple beams using a beam splitter within a single laser–scanner system. The intended application is the simultaneous processing of hybrid additively manufactured parts in high-volume production, using 3D optical systems with large, fully overlapping scan fields. Developing such a system requires a clearer understanding of the potential and trade-offs associated with manufacturing multiple parts simultaneously using a single laser–scanner system. To lay the groundwork for this approach, the present paper investigates the resulting build quality and the influence of optical-error mitigation strategies. The paper first describes the laboratory system and the compensation strategies, then presents and discusses their effects on the assessed build quality characteristics.

Materials and methods:

The presented experiments are conducted on a self-build laboratory test stand, as depicted in Figure 1, using a continuous wave near-infrared fiber laser with a wavelength of 1070 nm and a spot diameter on the build plate of 72 µm. As a material 316L stainless steel is used to build samples with an edge length of 10 mm in an argon shielding gas atmosphere at <0.3% oxygen. All samples are built with the same 175 W parameter set using a 30 µm layer height. The 3x1 beam splitter is realized using a diffractive optical element (DOE) positioned between the focusing unit and the scanner, resulting in a spot distance of 39.8 mm in the origin of the scanner coordinate system. Further, a custom slicer and machine control

developed within the research group are used to prepare the build jobs and to control the presented compensation strategies.

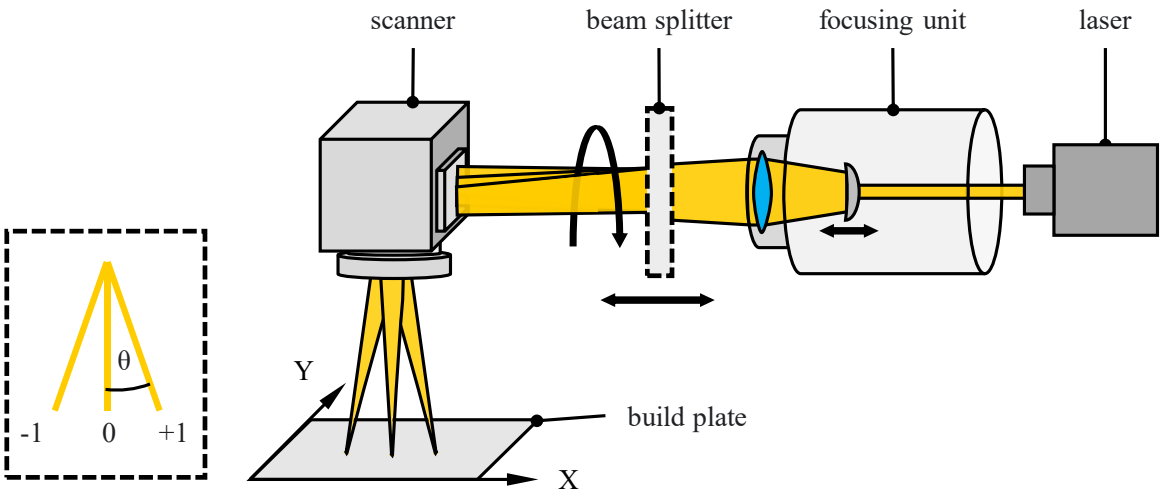


Figure 1: Overview of the laboratory test stand

The samples are scanned in a meander pattern, layer-wise alternating in directions, rotating 90 degrees. The positions of the samples are shown in Figure 2. Samples with the same number are scanned simultaneously, while the ones with the minus signs are processed by the side beam in the negative x-axis direction compared to the center beam, and vice versa for the ones with the plus signs. In this configuration, the spots of the beam splitter are oriented perpendicular to the shield gas flow and scanned against the direction of flow for the shield gas to minimize the influence of simultaneous upstream processed parts, which can impact build quality [30].

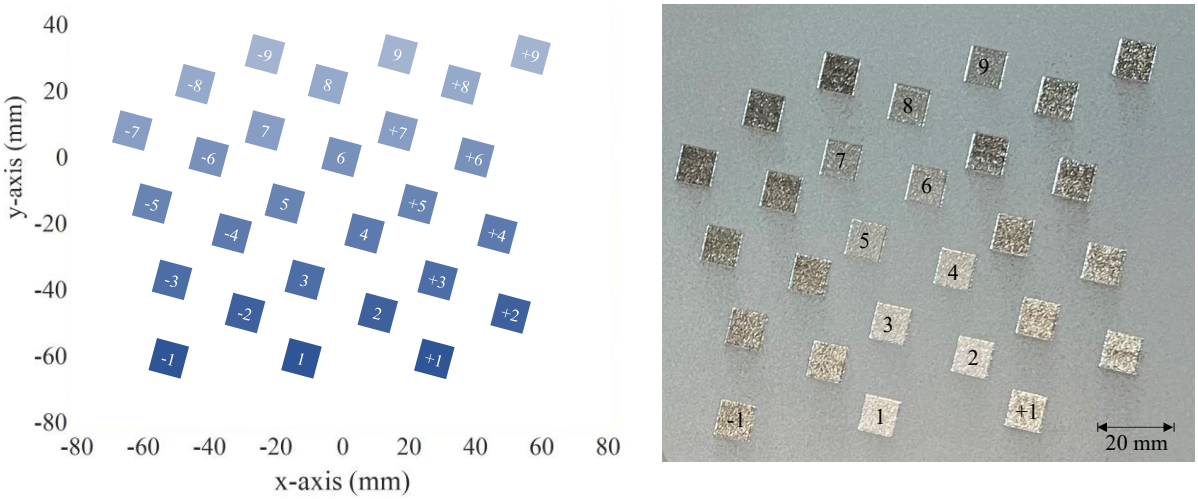


Figure 2: Sample positions and picture of the build job with beam splitter and no compensation

To determine the impact on the quality of the parts built in parallel, the properties of density, surface roughness, metallographic melt pool analysis, and position accuracy are investigated. Therefore, samples are separated from the build plate using wire-edm for buoyancy tests as well as polishing for metallographic analysis. The density measurements using the buoyancy method are conducted on a Sartorius LA310S scale with a measurement error of ±0.5 mg. To calculate the relative density, the highest measured value is taken as a reference for 100% density, which in this work is 7.958 g/cm³. Further, the surface roughness is measured using the Keyence VR 5000 white light interferometer. The values represent 30 line measurements equally distributed over each side of the sample except for the bottom of the sample, 15 horizontally and 15 vertically on every side. The metallographic analysis

consists of cutting the samples in the middle, perpendicular to the vectors on the top layer, and subsequently polishing them for metallographic density analysis. Further, the specimens are etched with V2A etching agent to allow for analysis of the melt pool geometries. The images are taken using the Keyence VHX 7000 digital microscope. Additionally, the geometrical deviations are investigated by the analysis of laser markings on anodized aluminium, processed with a digital microscope. This reveals the position errors without the influence of powder and melt pool.
To get an optical measurement of the actual focus error for every side sample and target sample, focal rows are marked on anodized aluminium. They consist of multiple parallel lines scanned with increasing focus offsets. Subsequently these markings are processed by image capture via a digital microscope and analysed with an image processing algorithm. This way the evaluation of the focal rows is done using the same criteria. An indicator for the resolution of this approach is achieved by using the single beam to mark 27 focal rows on the whole build plate and evaluating them with the same method, resulting in a measured standard deviation of 0.27 mm. Further, the peak intensity is measured using an LBP2 beam camera from Ophir. There the brightness setting of the camera is fixed in the focus of the single laser beam. Afterwards the split beams are measured, and the brightness counts of the pixels are considered the intensity. The maximum value of every defocus and beam combination is considered the peak intensity in this work. To gain further understanding of the process conditions, the laser power is measured individually for the split beams with an aperture and a Newport 919-250 power meter with a measurement accuracy of ±3%.

Compensation strategies

According to previous research, the PBF/LB-M process with a beam splitter is impacted by optical errors due to three-dimensional positioning errors of the focus spot depending on the target position and order of the beam [31]. This results in position dependent differences in spot sizes, and distances between the beams on the build plate. To simulate these inherent optical errors, a vector-based model was proposed by Spieth, Heeling, and Möhring. In their approach, the laser beams generated by a DOE are represented as vectors and traced through the optical system. The vectors are reflected by the galvo scanner mirrors according to their actual rotational angles and positions relative to the build plate. Consequently, the model enables the simulation and quantification of macroscopic inherent optical errors, which are categorized into spot distance error, rotation error, and focus error. The spot distance error describes the variation in distance between the outer beams and the center beam compared to the spot distance in the origin of the scan field. The rotation error quantifies the angular difference of the beam triplet relative to its reference orientation at the center of the scan field. Finally, the focus error represents the relative increase in the focus diameter compared to the focus diameter of the center beam at the scan field origin. [32] The application of the model in this study resulted in a maximum deviation of measured and simulated spot distance error of 0.039 mm as well as a 0.17° difference for the rotation error.
In the following, such a model is used to investigate compensation strategies for the optical errors. For the compensation of the optical errors, the spot distance errors are predicted and utilized to determine an optimal DOE position along the beam. Therefore, the DOE is translated along the optical beam path within a 30 mm interval towards the build plate, and the spot distance error is evaluated at 1 mm increments using the vector-based model. The position that minimizes the maximum spot distance error across all side beams is selected as the compensation position. Furthermore, rotation errors originating from non-orthogonal galvo mirror axes are compensated by applying an angular offset to the DOE, thereby counter rotating the beam pattern about the optical axis.
Compensation strategies for focus errors can be classified according to two degrees of freedom. The first concerns the compensation approach. Passive compensation refers to strategies in which the compensation parameters remain constant throughout the entire build job and are applied uniformly across all target positions. In the present work, passive compensation is realized through the selection of an optimized DOE featuring relative laser powers of 116% and 111% for the -1 and +1 side beams, respectively, compared with 87% and 82% for the conventional DOE. In contrast, active compensation involves adjusting the compensation parameters laser power and defocus individually for each target position. Within the scope of this work, two distinct optimization targets are investigated for the active compensation. The first optimization target, referred to as active focus compensation, involves defocusing the laser beam entering the DOE to minimize the maximum focus error within the beam

triplet. Therefore, as in the optimization of the spot distance error, the focus errors of all three beams are simulated across the adjustment range of the focusing system on increments of 0.1 mm. The focus offset that minimizes the maximum focus error among the three beams is selected as compensation offset. However, the second objective, referred to as active peak-intensity compensation, combines defocusing with an increase in laser power to minimize the maximum peak-intensity deviation of the three beams from the center beam at the scan-field origin. This procedure comprises two steps. First, the measured peak intensities of all three beams above and below the focal plane are used to select the focus offset that minimizes the maximum deviation from the measured peak intensity of the center beam at the scan-field origin. Second, assuming a linear relationship between laser power and peak intensity, the laser power is increased at the selected focus offset until the calculated minimum peak intensity is equal to the one of the center beam in the origin of the scan field. However, this compensation is limited by the maximum available laser power. Nevertheless, this strategy enables a first investigated to assess the effect of introducing laser power as an additional optimization variable for the compensation of position dependent optical errors, when deploying a DOE.

Results and discussion:

The potential of the presented compensation approaches is evaluated through a model-based investigation is conducted into the compensation of the spot distance-and rotation error. Furthermore, an experimental investigation is conducted for the purpose of examining of the focus error compensation. The results of the sample-building experiments are presented and discussed separately for every defined aspect of build quality, such as density and roughness. Furthermore, a qualitative comparison is made between the microstructure and melt pools of the samples and the results of metallographic analysis for the different compensation strategies. The objective of this study is to ascertain the experimentally accessible potential for compensation of build quality differences from optical errors

Spot distance- and rotation error

The evaluation of the compensation capabilities for reducing the position deviation from rotation error and spot distance error is conducted by fitting a rotatory and translatory axis to the test stand. This setup offers the possibility to make laser markings on aluminium plates with adjustable spot rotations and distances. In this case, the compensation for the build jobs presented in Figure 2 results in a reduction of the maximum spot distance error from 0.16 mm to 0.06 mm, while the average spot distance error decreases from 0.05 mm to 0.03 mm. In order to investigate the capabilities of the position compensation strategy for larger scan fields, simulation results with and without compensation for a build job with a 100 mm offset in the positive x-direction are presented. This offset results in increased position deviation from larger rotation and spot distance errors. In this instance, the range of spot distance errors is from 0.25 mm to 1 mm when operated without compensation, as illustrated in Figure 3. With the use of a translative compensation by adjusting the position of the beam splitter for every sample position, this spot distance error can be reduced to below 0.3 mm. This indicates a substantial reduction in the variability of the spread between all samples of a build job for the spot distance error, from 0.5 mm down to below 0.1 mm. This results in a more homogeneous spot error distribution over the build job, in addition to the overall lower maximum errors.

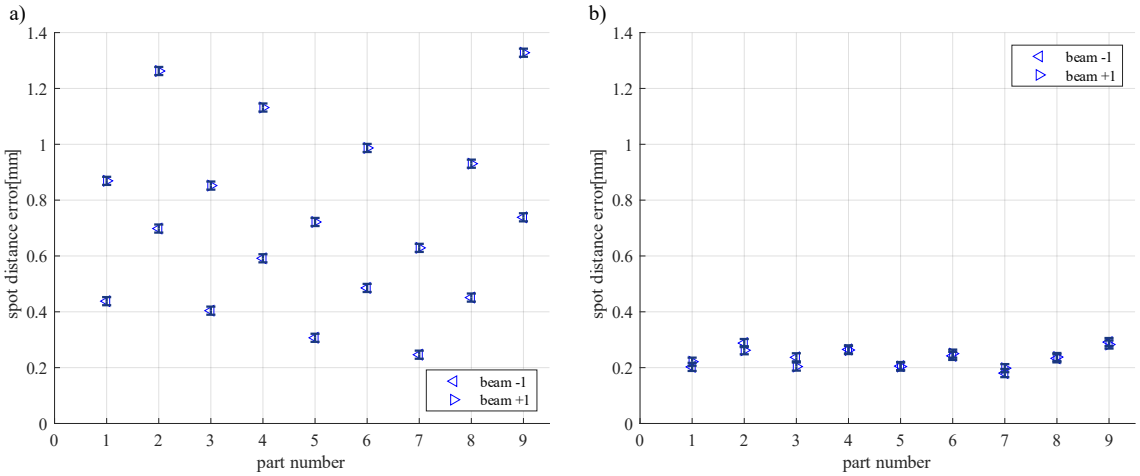


Figure 3: Spot distance error for a build job with a 100 mm offset in positive x-direction a) without compensation and b) with compensation from the translatory axis

For the rotation error, a full compensation is possible by counterrotation of the beam splitter to the rotation error around the center beam. Even for larger scan fields, this results in a reduction of the rotation error from up to 0.6° down to 0.0°, as depicted with the results of a simulation in Figure 4 for a build job with a 100 mm offset in the positive x-direction. With the main limitations for this compensation coming from the dynamic and accuracy of the rotation axis, this approach provides an effective compensation for the rotation error.

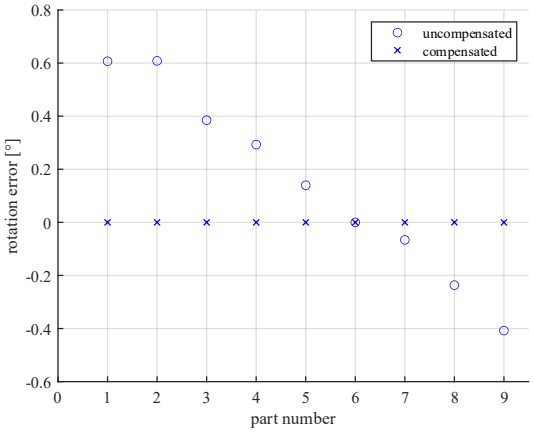


Figure 4: Simulated rotation error for a build job with a 100 mm offset in positive x-direction a) without compensation and b) with compensation from the rotatory axis

Density

The density of the build parts is investigated; to gain an understanding of the influence of different compensation strategies. In this case, the deviations from the focal length of the beam to the actual beam length to the build plate are considered the main influence on the density. This focus error is increasing porosity through changes in the energy distribution over a larger spot size and density of the process. Therefore, the goal for the compensation is to equalize the differences in density resulting from the remaining focus error and thereby working positions in the process window. Thus, the density values measured by the buoyancy method of all samples on the build plate for every tested compensation strategy are depicted in Figure 5. The samples produced without compensation show the largest spread, from 99.7% to 96.9%, and the lowest average density of 98.3%, which highlights the need for compensation to use beam splitting for printing multiple parts with one laser-scanner system. Yet the average densities of the compensated samples are close together, ranging from 99.5% to 99.4%. Nevertheless, the passive and the combined active and passive compensation strategies reveal a smaller spread in results than the active compensation-only strategy. However, the active compensation still highlights the potential for significant improvements in density. Yet a larger spread in density in between

the samples remains, and high laser powers are necessary to reach the peak intensities of the single beam process. Remarkably, the passive compensation via a model-based optimized beam splitter shows great improvements compared to the active-only and no compensation strategies, while not requiring online adjustments during the process. Still, the combined active and passive compensation strategies are measured with the highest minimum density, which is the most important factor aiming for process stability in a later industrial application. Thereby leading to the smallest deviations from the parameters of the single beam process. To allow for better comparability of the influences, all compensation strategies have been conducted with the same parameter set. Tested with a single laser beam, the parameter set resulted in an average density of 99.0% density. This parameter set is chosen because of its presumable high sensitivity to the expected optical errors and compensation strategies.

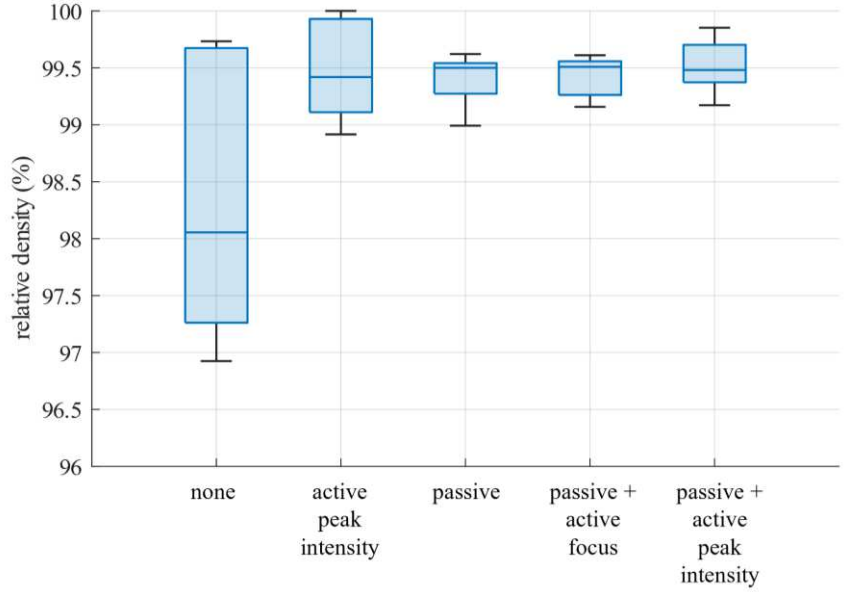


Figure 5: density distribution for the different compensation strategies

A more thorough examination of the density results reveals further insights by which the density increases due to the compensation. A more detailed view separated by relative laser power, defocus, and relative peak intensity, shows the main levers for compensation, as depicted in Figure 6. In this study the term relative is employed to describe the measured relative increase or decrease of laser power and peak intensity in comparison to the single-beam process. As illustrated by the red markings indicating the side beams, a clear trend can be observed, demonstrating an increase in minimal density with an increase in relative laser power. Although the densities of the center beam samples are high for all strategies, a comparable tendency is evident in the densities of samples constructed by the center beam, yielding densities ranging from 99.5% to 100%. However, samples that are uncompensated and have a relative laser power lower than 100% demonstrate the lowest densities, with a minimum of under 97% relative density. The discrepancy in minima between the density of side beam build and center beam build decreases with increasing laser power. The defocus of the individual samples is characterized by more subtle effects. The density results of the center beam demonstrate a high level of robustness against focusing below the working plane of the test stand, as evidenced by a comparison of the active and passive compensation strategies. The samples constructed by the center beam demonstrate the highest densities, even for larger defocus. This phenomenon is most likely attributable to the relatively modest sensitivity of the process to an augmentation of the beam diameter, given the Rayleigh length of 3 mm. Conversely, the density over defocus demonstrates a considerable impact on the densities of the uncompensated side beam samples. For samples built with active peak intensity compensation strategy, the laser power limitation, given by the test stand, could explain the density results below 99%, even though the side beams were in focus. However, it is important to note that solely reducing the focus error or the laser power differences is not the effective approach, as there are comparable low densities present within the samples of the actively compensated ones, as well as the passively compensated ones. When considering the combination of defocus and laser power in the form of peak intensity, a

correlation of increasing density with increasing peak intensity is visible. In the experiments with the highest average densities, the differences between the relative peak intensities for the center and side beams are minimal. This is particularly evident when comparing the results for combined compensation strategies with those for active or passive compensation strategies only. Demonstrating the impact of combined compensation, as this reduces the maximum discrepancies observed in the single-beam process through defocus, in addition to adjustments in the relative laser power per beam.

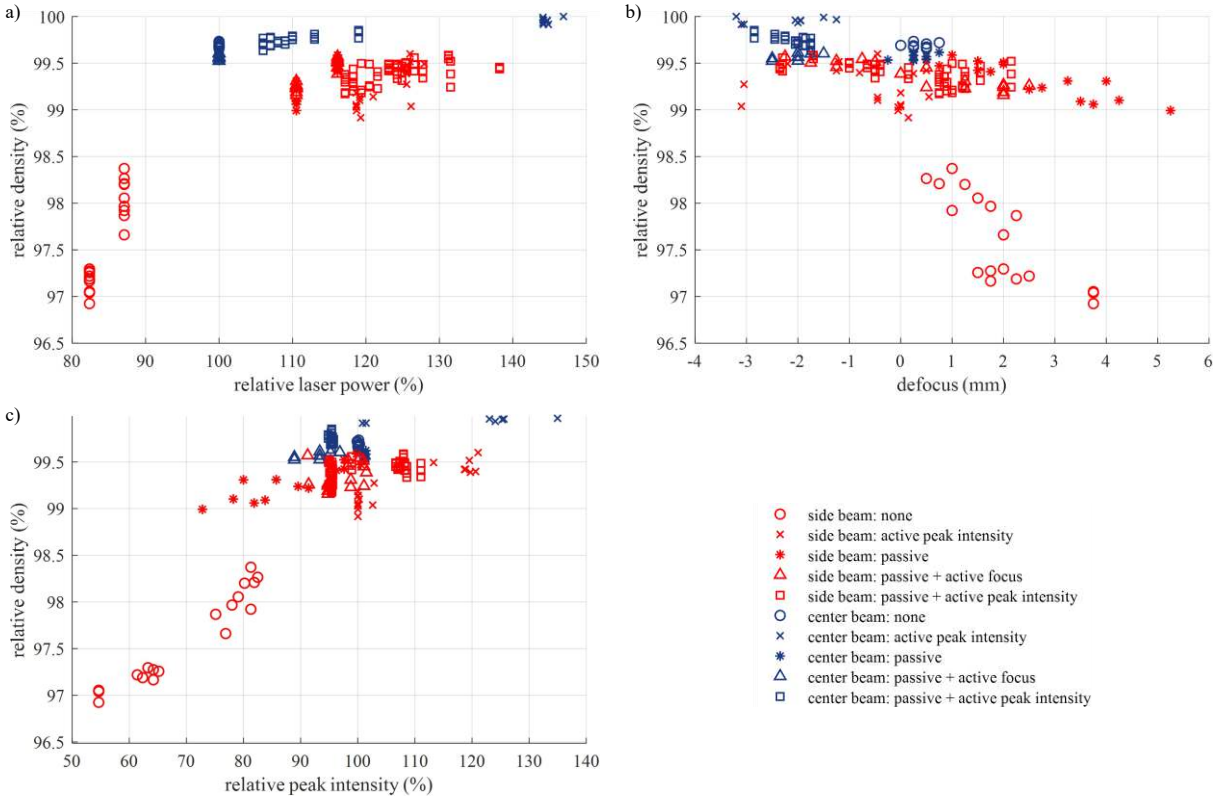


Figure 6:measured relative densities over a) relative laser power, b) defocus and c) relative peak intensity

As depicted in Figure 7, the samples built by the center beam show the highest densities. The densities reached with the side beams increased strongly with the use of compensation. While the left beam shows similar densities for the different compensation strategies, the right beam shows increasing densities for compensations with decreasing differences in peak intensity compared to the single beam process. This is due to an offset of the scanner origin compared to the origin in the experiments, which leads to larger focus errors for the samples built by the order +1 beam. Further, the samples of the right-side beam show a larger deviation in density compared to the ones built by the center beam and the left beam. A reason for this behaviour could be the overall lower peak intensity and thereby larger difference to the single beam process due to remaining non-compensatable errors.

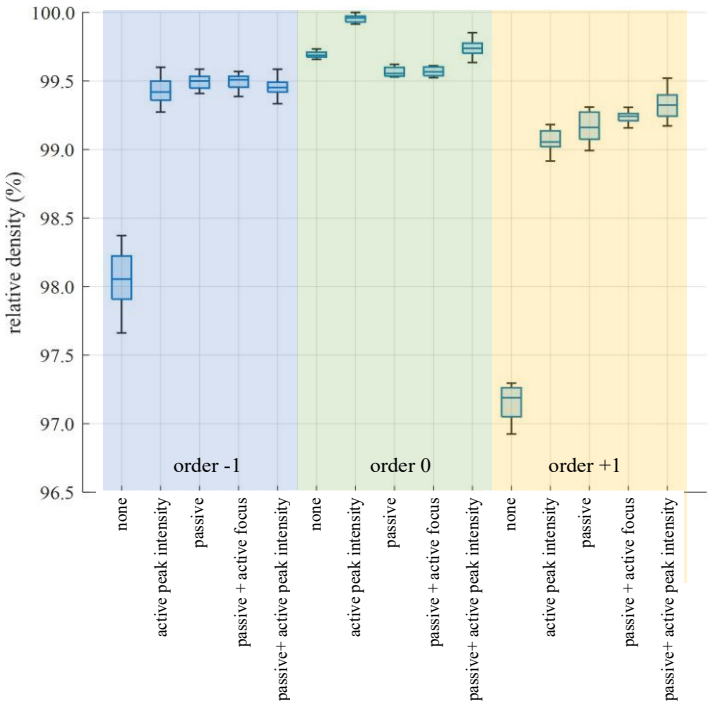


Figure 7: density for the different beams and compensations

Surface roughness

Furthermore, the surface roughness of the build specimen is investigated for the different compensation strategies. The mean values for the uncompensated side surface roughness are 11.9 µm, and the mean values for the combined passive and active peak compensation for the top surface roughness are 12.4 µm, as illustrated in Figure 8. However, it should be noted that the deviations are relatively similar for all compensation strategies, with the exception of the active peak intensity. In this instance, it is probable that the increase in laser power resulted in a process with sporadic adhesion of additional spatters to the surface. Concurrently, the wider weald beads served to reduce the roughness by increasing the overlap of weald beads, a phenomenon that might account for the observed deviations in roughness for this compensation strategy.

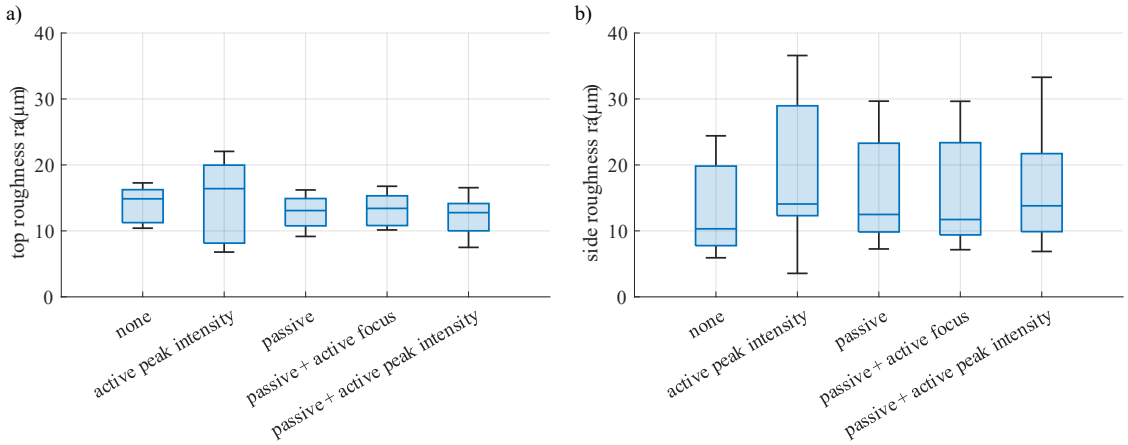


Figure 8: surface roughness for the different compensation strategies on a) the top surface of the sample and b) the sidewall

As depicted in Figure 9, the samples constructed using the center beam exhibited a reduced overall top surface roughness in comparison to the side beams. Furthermore, the side beams of the active peak intensity compensation strategy result in higher top surface roughness compared to the other compensation strategies. For the side wall roughness, the samples built by the side beams demonstrated a higher degree of deviation compared to the samples built by the center beam. The phenomenon may be attributed to the increased beam diameter resulting from defocus. In the case of a gaussian-like beam,

the elevated sidewall roughness is primarily attributable to the partial melting of surrounding powder, caused by the lower gradients in the intensity profile's edge region.

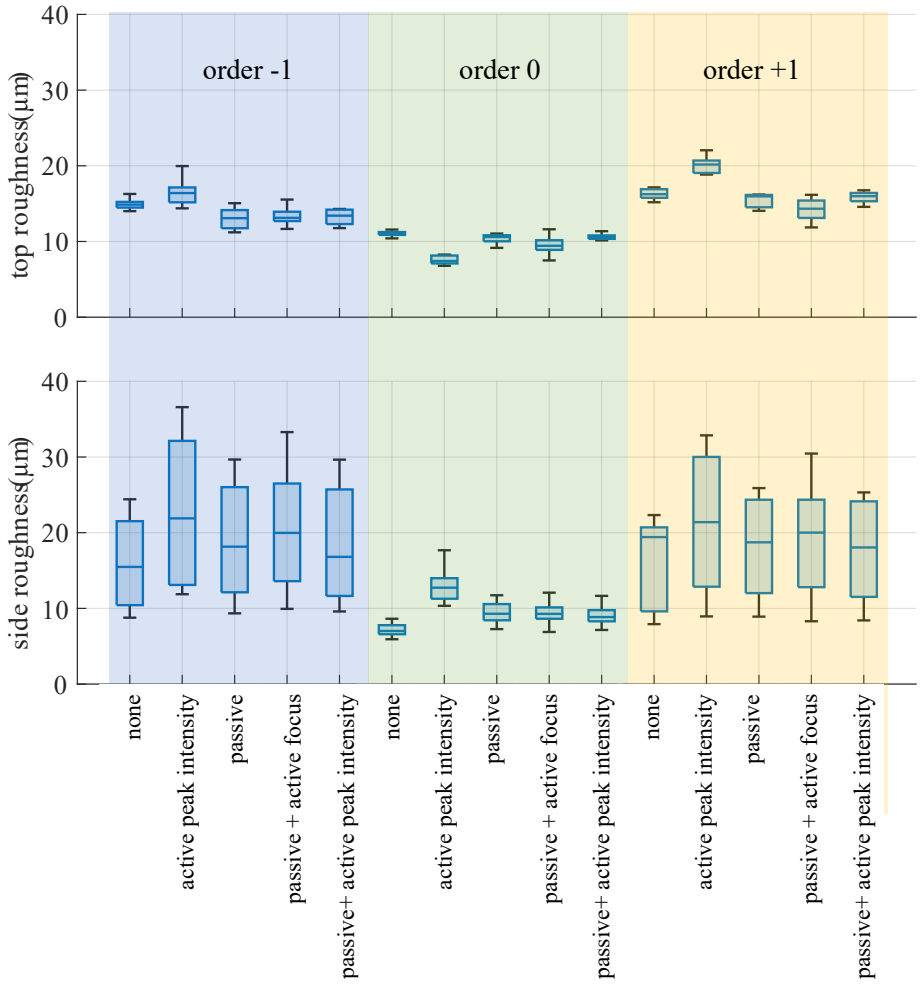


Figure 9: surface roughness separated by beams and compensation strategies

The top surface roughness appears to be influenced by the various compensation strategies, as illustrated in Figure 10. A decrease in roughness is measured for the higher laser power build samples of the center beam with only active peak compensation. This phenomenon may be attributed to an increase in the diameter of the melt pool, which results in an increase in the overlapping area between vectors smoothing roughness. In contrast, higher roughness measurements were recorded for the upper surfaces of the active peak-compensated side beam build samples. This is attributed to the inability of defocus and laser power adjustments to reach sufficient energy densities in the side beams, thereby leading to lack of fusion on the top surface of the samples. This effect is most likely the result of powder attachments to the sides of the samples built with higher laser power densities in the edge areas of the beam from power increases through active or passive compensation combined with the defocus of the side beams.

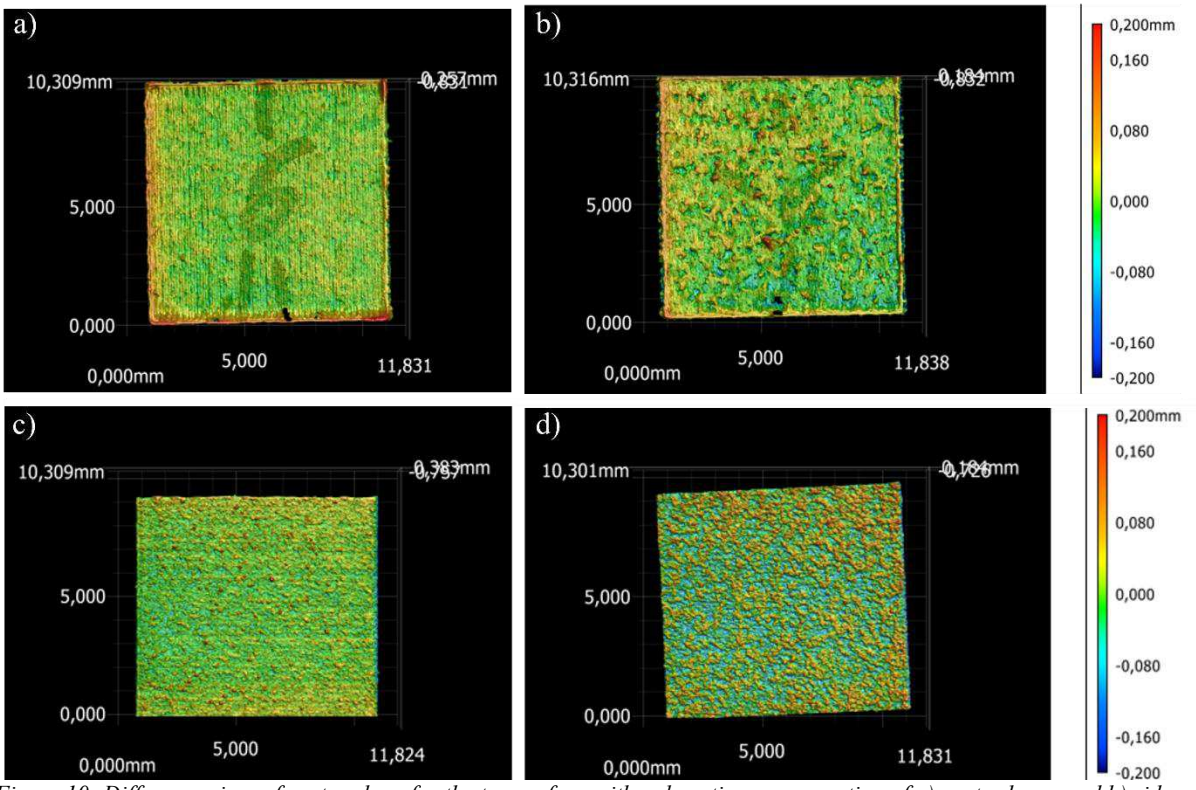


Figure 10: Differences in surface topology for the top surface with only active compensation of a) center beam and b) side beam as well as the side walls for c) center beam and d) side beam

Metallographic analysis

Additionally, the samples are analysed by metallographic analysis as depicted in Figure 11. There a change of the melt pool geometry is visible. While the non-compensated side samples show large pores due to lack of fusion from lower laser power as well as a defocus in the side beams compared to the center beam, with an increase of the energy from the laser beam from passive compensation, a decrease of pores is visible. In this compensation configuration, the melt pools of the side beams are wider, likely due to the combination of higher laser power and defocus in the side beams from the tailor-made DOE and differences between focal length and actual length to the build plate. With combined compensation through additional active peak intensity optimisation, further increases in energy density result in even lower amounts of pores in the samples built by the side beams, as well as a harmonisation of the melt pool geometries of the center and side samples. Now deeper investigation of the influence of peak intensity on the metallographic results is done in the next step, where the changes in peak intensity for the side beams are shown for similar focus positions and similar power levels. Different parameter sets can lead to dense samples due to the interaction of the weld beads with the previously scanned weld beads. Nevertheless, in these experiments only one parameter set has been investigated. Adjusting the beams to a similar focal diameter and peak intensity compared to the center beam makes the weald beads of the side beams similar to the ones of the center beam. This difference remains across all experiments and compensations. With the compensation also the similarity between the different sample positions is increased. Yet a residual difference between the ones with the highest focus error and the ones with the lowest remains. This effect can be attributed to the single lever for all beams compensation strategy, because every sample position is part of a triple of positions, focus- and power levels.

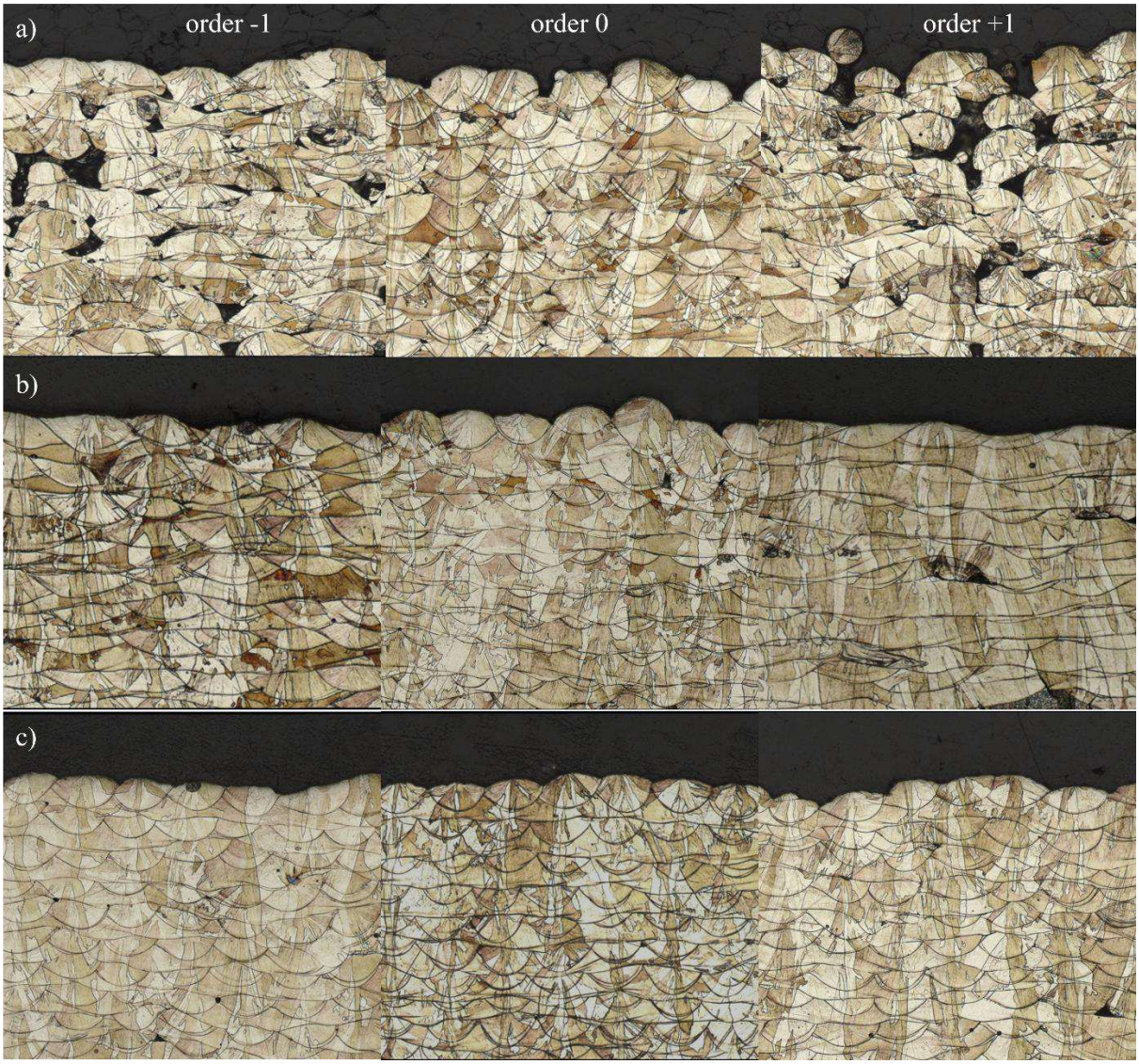


Figure 11: Metallographic microscopy of the top layer from etched samples with different compensation approaches a) none, b) passive and c) combined passive and active compensation

As visible in Figure 12, compensation strategies close the gap to the peak intensity of the single beam process, resulting in lower porosities. Many of the small lack of fusion pores in between weld beads are present for the samples without compensation. While with increasing equalisation the smaller pores vanish almost completely, a few larger pores remain and become more pronounced even for the combined active and passive compensations. These remaining pores are expected to be the result of spatter reattaching to the build specimen, most likely due to their higher mass resulting in less effect of the shield gas flow. In conclusion, these results show a possibility for partial compensation of the build quality disadvantages from the focus errors.

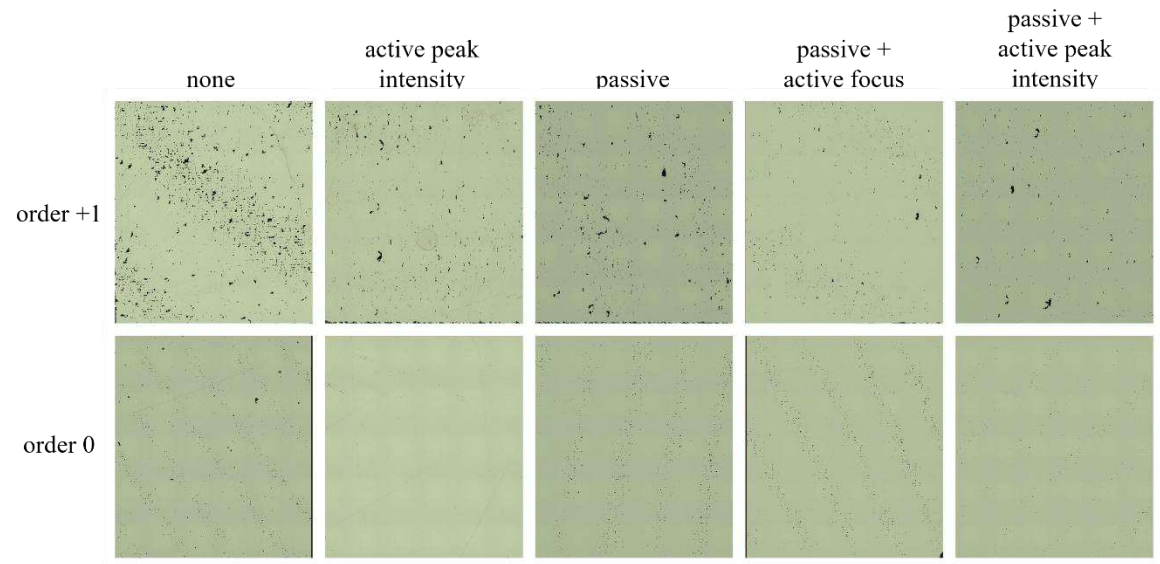


Figure 12: Metallographic image of the full sample before etching for the different compensation strategies

Conclusion & Outlook:

This paper presents the influence of compensation strategies on using a beam splitter to build multiple same parts in parallel with one laser scanner system. The new approach demonstrates the possibility for an increase in productivity by multiplying a power-limited single-beam process. Furthermore, the influence of error reduction on the quality of parts built simultaneously is investigated for the characteristics density, surface roughness and metallographic analysis. Therefore, the compensation of spot distance- and rotation errors are analyzed. Additionally, multiple compensation strategies are tested experimentally for the compensation of the focus error, and the resulting build qualities were analyzed. The main takeaways are as follows:

- Simulations predict a 70% reduction in spot-distance error for the use of compensation by target position dependent positioning of the beam splitter along the laser beam
- Rotation errors are fully compensable, by counterrotation of the beam splitter about the beam
- Experimental evaluation shows an increase in average build density from 98.3% to 99.5% on build job level by compensation
- Compensation improves homogeneity of build quality by reducing sample to sample variability

Therefore, the investigated compensation approaches enhance positioning accuracy and promote more consistent build quality on build job level. The experimental results indicate that the selected compensation approaches provide promising initial results while still showing potential for further error reduction. In future experimental studies, the focus should be on the combined use of compensation methods as well as expanding the investigation into additional build quality characteristics. Further development of build-job preparation is required to account for constraints imposed by the shielding-gas flow direction and the compensation requirements. Addressing these issues could support the production of parts with more consistent quality tailored to application-specific requirements and foster the potential use of this process in series production of additive manufactured parts by introducing process scalability by available laser power.

References

[1] Yang, J., Li, B., Liu, J., Tu, Z., Wu, X., 2024. Application of Additive Manufacturing in the Automobile Industry: A Mini Review. Processes 12 (6), 1101. doi:10.3390/pr12061101.

[2] McConnell, S., Tanner, D., Kourousis, K.I., 2024. Productivity improvement opportunities for metal powder bed fusion technologies: a systematic literature review. RPJ 30 (11), 230–245. doi:10.1108/RPJ-09-2023-0333.

[3] Laureijs, R.E., Roca, J.B., Narra, S.P., Montgomery, C., Beuth, J.L., Fuchs, E.R.H., 2017. Metal Additive Manufacturing: Cost Competitive Beyond Low Volumes. Journal of Manufacturing Science and Engineering 139 (8). doi:10.1115/1.4035420.
[4] Wohlers, T.T., ASTM International, 2024. Wohlers Report 2024: 3D Printing and Additive Manufacturing : Global State of the Industry. Wohlers Associates.
[5] Manoj Kanskar, Scott Keeney, Robert Martinsen. Laser Diodes: The power of brilliance — the past and future of high-power semiconductor lasers. https://www.laserfocusworld.com/lasers-sources/article/16555251/laser-diodes-the-power-of-brilliance-the-past-and-future-of-high-power-semiconductor-lasers.
[6] Wang, P., Robertson, G., Gibson, B.T., Fancher, C.M., Reynolds, J., Borish, M., Cruz, J.R., Chesser, P., Stump, B., Jackson, A., MacDonald, E., 2024. Improved Productivity with Multilaser Rotary Powder Bed Fusion Additive Manufacturing. 3D printing and additive manufacturing 11 (1), 231–241. doi:10.1089/3dp.2022.0288.
[7] Zhao, L., Zhang, J., Yang, J., Hou, J., Li, J., Lin, J., 2024. Microstructure and mechanical properties of 316L stainless steel manufactured by multi-laser selective laser melting (SLM). Materials Science and Engineering: A 913, 147053. doi:10.1016/j.msea.2024.147053.
[8] Pfalz, T., Rota, A., Saeidnezhad, N., Leyens, C., 2023. Comparison of different multi-laser powder bed fusion exposure strategies and their influence on the part quality of IN718. Int J Adv Manuf Technol 128 (9-10), 4469–4490. doi:10.1007/s00170-023-12194-3.
[9] Li, S., Yang, J., Wang, Z., 2021. Multi-laser powder bed fusion of Ti-6.5Al-2Zr-Mo-V alloy powder: Defect formation mechanism and microstructural evolution. Powder Technology 384, 100–111. doi:10.1016/j.powtec.2021.02.010.
[10] Heeling, T., 2018. Synchronized Two-Beam Strategies for Selective Laser Melting. dissertation, Zurich. doi:10.3929/ethz-b-000270330.
[11] Zhang, W., Hou, W., Deike, L., Arnold, C.B., 2020. Using a dual-laser system to create periodic coalescence in laser powder bed fusion. Acta Materialia 201, 14–22. doi:10.1016/j.actamat.2020.09.071.
[12] Liu, Z., Song, C., Han, X., Xiao, Y., Liu, K., Yang, Y., 2023. Effect of dual-laser powder bed fusion on surface quality, internal defects and properties of 316L stainless steel. Journal of Materials Research and Technology 27, 5681–5691. doi:10.1016/j.jmrt.2023.10.221.
[13] Tenbrock, C., Kelliger, T., Praetzsch, N., Ronge, M., Jauer, L., Schleifenbaum, J.H., 2021. Effect of laser-plume interaction on part quality in multi-scanner Laser Powder Bed Fusion. Additive Manufacturing 38, 101810. doi:10.1016/j.addma.2020.101810.
[14] Grünewald, J., Gehringer, F., Schmöller, M., Wudy, K., 2021. Influence of Ring-Shaped Beam Profiles on Process Stability and Productivity in Laser-Based Powder Bed Fusion of AISI 316L. Metals 11 (12), 1989. doi:10.3390/met11121989.
[15] Lantzsch, T., Heussen, D., Praetzsch, N., Häfner, C., 2022 - 2022. Evaluation of productivity scaling approaches for laser powder bed fusion of nickel-base alloy 625, in: High-Power Laser Materials Processing: Applications, Diagnostics, and Systems XI. High-Power Laser Materials Processing: Applications, Diagnostics, and Systems XI, San Francisco, United States. 22.01.2022 - 28.02.2022. SPIE, p. 5. doi:10.1117/12.2611151.
[16] Chechik, L., Schwarzkopf, K., Rothfelder, R., Grünewald, J., Schmidt, M., 2024. Material dependent influence of ring/spot beam profiles in laser powder bed fusion. Additive Manufacturing Letters 9, 100211. doi:10.1016/j.addlet.2024.100211.
[17] Laskin, A., Volpp, J., Laskin, V., Nara, T., Jung, S.R., 2021. Multispot optics for beam shaping of high-power single-mode and multimode lasers. Journal of Laser Applications 33 (4). doi:10.2351/7.0000461.
[18] Slodczyk, M., Ilin, A., Kiedrowski, T., Bareth, T., Ploshikhin, V., 2021. Spatter reduction by multi-beam illumination in laser powder-bed fusion. Materials & Design 212, 110206. doi:10.1016/j.matdes.2021.110206.

[19] Wischeropp, T.M., Tarhini, H., Emmelmann, C., 2020. Influence of laser beam profile on the selective laser melting process of AlSi10Mg. Journal of Laser Applications 32 (2). doi:10.2351/7.0000100.
[20] Schleifenbaum, H., Diatlov, A., Hinke, C., Bültmann, J., Voswinckel, H., 2011. Direct photonic production: towards high speed additive manufacturing of individualized goods. Prod. Eng. Res. Devel. 5 (4), 359–371. doi:10.1007/s11740-011-0331-0.
[21] Brudler, S., Medvedev, A.E., Pandelidi, C., Piegert, S., Illston, T., Qian, M., Brandt, M., 2024. Systematic investigation of performance and productivity in laser powder bed fusion of Ti6Al4V up to 300 µm layer thickness. Journal of Materials Processing Technology 330, 118450. doi:10.1016/j.jmatprotec.2024.118450.
[22] Lantzsch, T., Westphalen, T., Tenbrock, C., Traub, M., Haefner, C.L., 2021. Laser Powder Bed Fusion of Stainless Steel 316L Using a Flexible Dual Fiber Laser Array, in: 2021 International Solid Freeform Fabrication Symposium, Austin. doi:10.26153/tsw/17671.
[23] Tsai, C.-Y., Cheng, C.-W., Lee, A.-C., Tsai, M.-C., 2019. Synchronized multi-spot scanning strategies for the laser powder bed fusion process. Additive Manufacturing 27, 1–7. doi:10.1016/j.addma.2019.02.009.
[24] Yu, K.-S., Cheng, C.-W., Lee, A.-C., Jhang Jian, W.-Y., Chang, W.-C., Chang, T.-W., Tsai, M.-C., 2022. Additive manufacturing of NdFeB magnets by synchronized three-beam laser powder bed fusion. Optics & Laser Technology 146, 107604. doi:10.1016/j.optlastec.2021.107604.
[25] Cirakoglu, K., Holder, D., Richmond, A., Flamm, D., Grossmann, D., Sutter, D., Hagenlocher, C., Graf, T., 2024. Simultaneous micromachining with beam splitting of ultrashort laser pulses at high average power for the productive fabrication of microchannels. Procedia CIRP 124, 708–711. doi:10.1016/j.procir.2024.08.207.
[26] Büsing, L., 2016. Optische Systeme für die hochpräzise, scannerbasierte Multistrahlbearbeitung mit ultrakurzen Laserpulsen. dissertation, Aachen.
[27] Hofmann, O., Stollenwerk, J., Loosen, P., 2020. Design of multi-beam optics for high throughput parallel processing. Journal of Laser Applications 32 (1), 12005. doi:10.2351/1.5125778.
[28] Nie, X., Chen, Z., Qi, Y., Zhang, H., Zhang, C., Xiao, Z., Zhu, H., 2020. Effect of defocusing distance on laser powder bed fusion of high strength Al–Cu–Mg–Mn alloy. Virtual and Physical Prototyping 15 (3), 325–339. doi:10.1080/17452759.2020.1760895.
[29] Liu, B., Fang, G., Lei, L., Liu, W., 2022. Experimental and numerical exploration of defocusing in Laser Powder Bed Fusion (LPBF) as an effective processing parameter. Optics & Laser Technology 149, 107846. doi:10.1016/j.optlastec.2022.107846.
[30] Spieth, F., Heeling, T., Moehring, H.-C. (Eds.), 2024. Process Limitation for Powder Bed Fusion with Laser Beam Multiplication. University of Texas at Austin.
[31] Spieth, F., Heeling, T., Moehring, H.-C., 2024. Beam multiplication for powder-based metal Additive Manufacturing – approach, design and evaluation. Procedia CIRP 124, 362–365. doi:10.1016/j.procir.2024.08.134.
[32] Spieth, F.J.O., Heeling, T., Möhring, H.-C., 2025. Model for optical errors using a beam splitter with high separation angle in powder bed fusion. Prog Addit Manuf 10 (10), 7979–7990. doi:10.1007/s40964-025-01087-4.